

DIAGNOSTICS FOR A HIGH EMITTANCE AND HIGH ENERGY SPREAD POSITRON SOURCE

N. Vallis^{1*}, F. Marcellini, R. Zennaro, M. Zykova,
 P. Craievich, R. Fortunati, R. Ischebeck, E. Ismaili, P. Juranic, G.L. Orlandi, M. Schaer
 Paul Scherrer Institute, Villigen, Switzerland
¹also at EPFL, Lausanne, Switzerland

Abstract

This paper is an overview of a diagnostics setup for highly spread e+e- beams, to be installed at the PSI Positron Production (P³ or P-cubed) experiment. To be hosted at the Swiss-FEL facility (PSI, Switzerland) in 2026, P³ is e+ source demonstrator designed to generate, capture, separate and detect nano-Coulombs of secondary e+ and e- bunches, in spite of their extreme transverse emittance and energy spread. The experiment will employ an arrangement of broadband pick-ups (BBPs) to detect simultaneously the time structure of secondary e+e- bunches. A spectrometer will follow the BBPs and deflect the e+ and e- onto two unconventional faraday cups that will measure their charge. In addition, the energy spectrum of e+ and e- distribution will be reconstructed through scintillating fibers.

INTRODUCTION

The SwissFEL facility [1] (PSI, Switzerland) will host the PSI Positron Production (P³ or P-cubed) experiment [2] in 2026, a e+ source demonstrator with potential to improve by an order of magnitude the present state-of-the-art e+ yield. The experiment layout is shown in Fig. 1, featuring a e+ source based on a 6 GeV electron (e-) beam and 17.5 mm-thick (or 5 times the radiation length) amorphous Tungsten target. A capture system will follow the target, consisting of a solenoid system and 2 RF accelerating cavities. The remarkable e+ capture capabilities of P³ are enabled to great extent by the usage of high temperature superconducting (HTS) solenoid around the target region, as well as a novel standing wave solution for the RF cavities that provides a large iris aperture to maximize e+ capture.

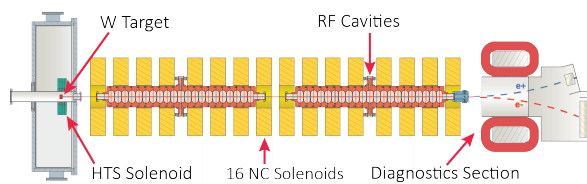


Figure 1: Simplified layout of the P³ [2].

The experiment diagnostics, whose layout is shown in Fig. 2, will be located directly downstream from the 2nd RF cavity, as illustrated in Fig. 1. This setup will measure the e+e- bunches before and after species separation, equipped with an arrangement of broadband pick-ups (BBPs), 2 Faraday Cups (FCs) and a variety of scintillating detectors. The

* nicolas.vallis@psi.ch

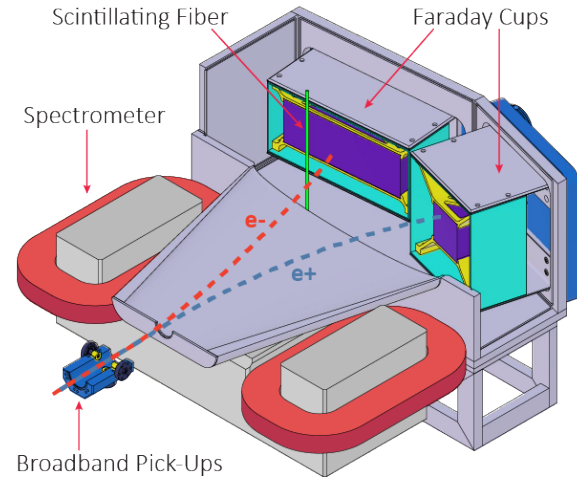


Figure 2: Concept design of the P³ diagnostics.

BBPs will detect, simultaneously for both particle species, the time structure of the captured e+e- bunches. The FCs and scintillators will be installed in the same vacuum chamber, and will measure the charge and energy spectrum of separate e+ and e- streams. Separation will be provided by a spectrometer, a dipole magnet based on four copper coils and an iron yoke, which will be fed at a maximum current of 340 A in order to reach magnetic fields up to 0.25 T. Additional diagnostics such as the arrangement of screens and cameras are still under discussion.

e+e- Dynamics in P³

200 pC e- at 6 GeV will impinge upon the 17 mm-thick Tungsten target, yielding a e+e- beam in the multi-MeV and nano-Coulomb range. Table 1 shows the evolution of the e+ bunches along the P³ capture line. These values clearly indicate that e+ dynamics are heavily dominated by an extremely high transverse emittance. In the transverse plane, e+ collection relies on the so-called Adiabatic Matching [3,4], a well-known e+ capture technique based on transforming the transverse phase space of newly generated e+ (moderate σ_x and large σ_{px}) into the acceptance of the capture line (large σ_x and moderate σ_{px}). Thus, emittance is not damped but matched and transported up to the diagnostics section. As for the longitudinal beam dynamics, RF fields will generate time structures of many consecutive e+ and e- bunches separated by the S-band $\lambda/2$ (167 ps or 50 mm in the ultrarelativistic regime), with the most particle population concentrated over the first two RF buckets. Two RF working points of interest

Content from this work may be used under the terms of the CC-BY-4.0 licence (© 2023). Any distribution of this work must maintain attribution to the author(s), title of the work, publisher, and DOI

Table 1: Main parameters of the e+ bunches for RF working points of interest. Simulated with ASTRA [5].

	$\Phi = (120, -70)$	$\Phi = (70, -110)$
Q_{e+} [pC]	1246	1155
σ_x, σ_y [mm]		7
σ_{px}, σ_{py} [MeV/c]		0.5
ϵ_{norm} [π mm mrad]		≈ 4000
σ_t [ps]		≈ 33
ΔE_{RMS} [MeV]	100	95

(see Fig. 3) were found in previous optimization studies: $\Phi = (120, -70)$, which provides maximum e+ capture and $\Phi = (70, -110)$, which will provide maximum energy compression [2]. The quality of measurements must therefore be particularly high for these RF phase configurations.

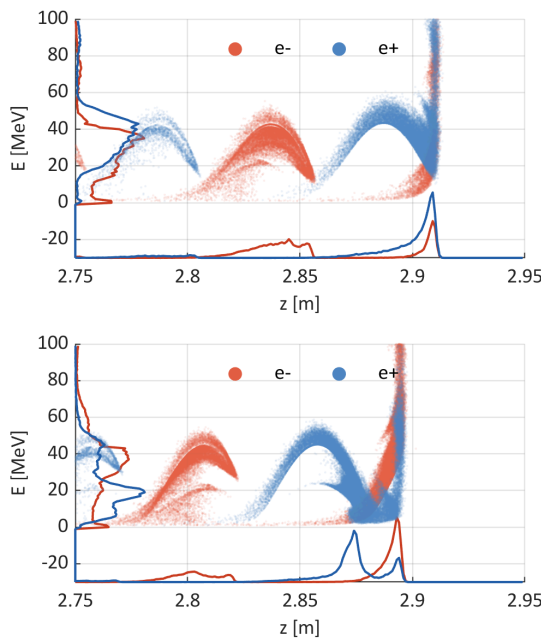


Figure 3: Simulated e+e- distributions near the exit of the 2nd RF cavity ($z \approx 2.8$ m) for RF working points of interest: $\Phi = (120, -70)$ (top) and $\Phi = (70, -110)$ (bottom).

SIMULTANEOUS e+e- DIAGNOSTICS: BROADBAND PICK-UPS

An arrangement of 4 broadband pick-ups (BBPs), shown in Fig. 4, will follow the second RF cavity and detect the wake voltage generated by the captured e+ and e- bunches. This will allow to reconstruct the e+ and e- time structure simultaneously, including measurements of charge, length and separation bunch by bunch. The e+e- time structure will heavily depend on the RF phase, yet the typical distribution will consist of alternating e+ and e- bunches of 33 ps length, and separated by 167 ps, namely half S-band period (see Fig. 3 and Table 1). Therefore, the geometry of the pick-ups

was optimized to avoid intrinsic resonances up to frequencies in the range of a few tens of GHz, while providing a relatively high peak voltage. According to a preliminary simulation based on a gaussian approximation of the P³ bunches (see Fig. 5), the BBPs would detect a ± 4.5 V peak voltage signal with very small distortion. Notice that this simulation does not take into account wakefield effects, cable distortion or environment noise.

Two BBP assemblies shown in Fig. 6 have been developed and fabricated, based on broadband feedthroughs of 27 GHz [6] and 65 GHz [7]. The hardware acquisition setup will consist of low attenuation, broad band cables [8] and a high-end oscilloscope of at least 40 GHz pass band and 10 GS/s sampling. Similar solutions based on ultra fast pick-ups are currently used in accelerator facilities such the fast BPMs at the SuperKEKB e+ linac [9, 10] and the Bunch Arrival-Time Monitors at SwissFEL [11].

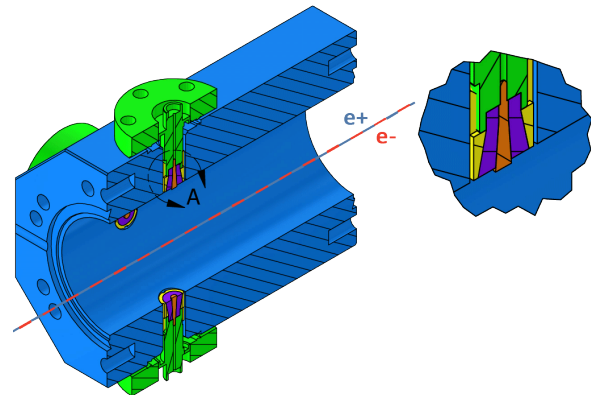


Figure 4: Mechanical design of the 27 GHz BBP assembly.

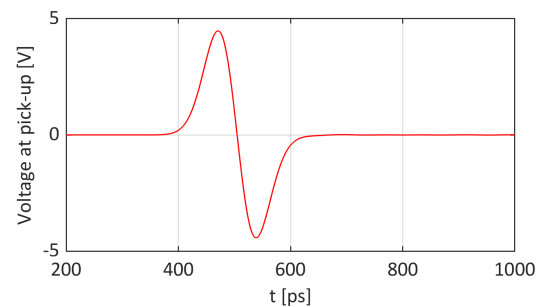


Figure 5: Detected voltage signal by one pick-up using 27 GHz feedthrough arrangement. Signal generated by gaussian bunch of $Q_{bunch} = 1$ nC and $\sigma_t = 33$ ps. Simulated with CST [12].

DIAGNOSTICS AFTER SEPARATION OF e+ AND e-

Faraday Cups

As illustrated in Fig. 2, the spectrometer will deflect the e+ and e- streams onto two faraday Faraday cups (FCs). Due to the extremely large energy (and p_z) spread, the main

challenge for both FCs is to collect a beam with a high transverse dispersion introduced at the spectrometer, for which each FC will follow a different principle. Note that both e+ and e- could be delivered to either FC through a sign inversion of the spectrometer polarity.

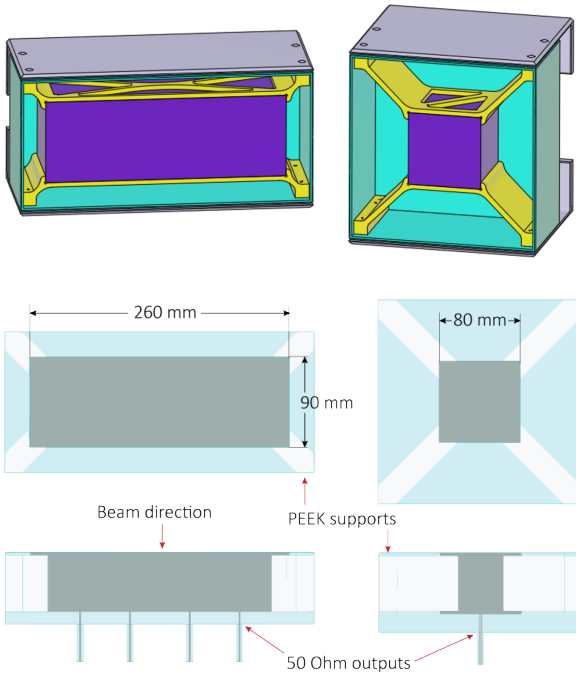


Figure 6: RF (top) and mechanical (bottom) design of 12.5 Ω (left) and 50 Ω (right) FCs, including tungsten blocks, PEEK supports and vacuum space.

The first FC is tuned at 12.5 Ω in pursuit of a large transverse area (260x90 mm), which will maximize the collection of charged particles in a wide energy range of 9-75 MeV. The coaxial impedance, a factor 4 smaller than the 50 Ω standard, can be easily matched to standard circuits through the use of parallel 4 coaxial cables. A second, relatively compact FC (80x80 mm) tuned at 50 Ω will detect charged particles in a larger energy range of 3-90 MeV. Although the smaller transverse size does not allow for single-shot charge measurements in broad energy spectra, the 50 Ω FC will perform energy discriminating measurements by adjusting the spectrometer strength, which determines the energy range of the particles routed towards the FC. A scan of 6 magnetic field values indicated in Table 2 would cover the above mentioned 3-90 MeV range. Figure 7 shows the frequency response of both FC arrangements with four diagonal PEEK supports (as seen in Fig. 6), in both cases above 1 GHz.

Error estimations of the measured e+ charge are shown in Fig. 8 for both FC layouts and all RF phase configurations, showing a reasonably low errors in the vicinity of the RF working point of interest. These error studies are based on ASTRA [5] particle tracking simulations. At $\Phi = (120, -70)$, the point for maximum captured e+ charge, the 12.5 Ω and 50 Ω FCs would read -13.6% and -9.4% with respect to the expected 1246 pC. 60 mm-thick W blocks were considered

Table 2: Reference spectrometer strength and measured energy ranges for different channels of FCs. Values based on zero-emittance particles.

	Mag. strength [T]	E. range [MeV]
12.5 Ω FC	0.053	9 - 75
	0.212	50 - 90
	0.120	28 - 50
50 Ω FC	0.068	16 - 28
	0.038	9 - 16
	0.021	5 - 9
	0.012	3 - 5

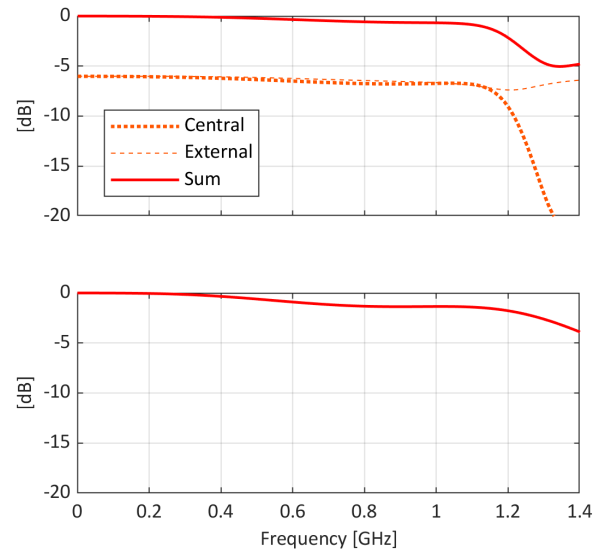


Figure 7: Frequency response of 12.5 Ω (top) and 50 Ω (bottom) FCs. Based on HFSS [13] simulations.

for both FCs in order to maximize charge deposition. Back scattering effects due to the high Tungsten density are disregarded as they are negligible above 10 MeV. On the other hand, poorer charge measurements are expected at lower energies, as particle divergence will have a greater impact in the final transverse position. However, this occurs in regions with relatively small importance for the experiment.

Scintillators in Diagnostics Chamber

Aside from the FCs, the diagnostics chamber will accommodate at least two additional instrumentation setups based on scintillator materials. First, the front face of the FCs will have scintillating screens that will allow cameras mounted outside of the chamber to look at the collected e+ and e- distributions. These scintillator screens are particularly useful during beam commissioning, as counterpart of the FC signals. However, the large size of the FCs and the transverse emittance of the beam result in a very poor energy resolution, which precludes any usefulness of performing spectral measurements through these devices. The scintillator can either be a coating deposited on the face of the FCs, a screen mounted to the front of the FCs, or a free-standing screen

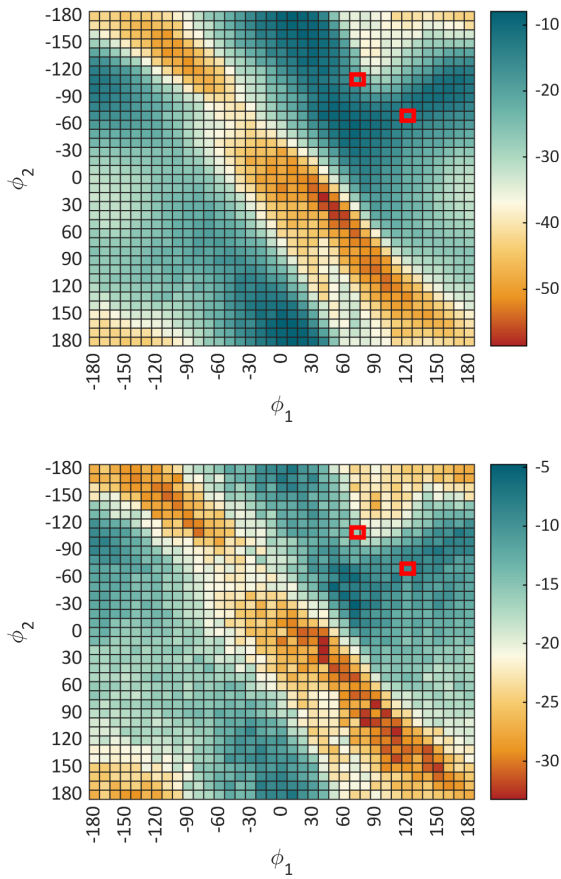


Figure 8: Error (in %) of measured charge by large 12.5 Ω (top) and compact 50 Ω (bottom) FCs over 2D RF phase scan. Estimated through particle tracking simulations with ASTRA [5]. $\Phi = (120, -70)$ and $\Phi = (70, -110)$ marked in red.

that can be inserted in and out of the chamber. The most likely materials for the screen would be Cr-doped Alumina (Chromox), Biomax, or YAG, which have been used for scintillation in accelerators in the past [14].

An high-resolution spectroscopic setup consisting of at least one pair of scintillator fibers will reconstruct the longitudinal momentum (p_z) spectrum of the e+ and e- distributions. The fibers, vertically oriented, will be hit by a small fraction of the particles corresponding to a narrow division of the energy spectrum. Following the basic principle of beam loss monitors, scintillator fibers will emit a signal proportional to the ionisation energy released by the incident charges. This will allow to scan the dipole field strength over as many points as desired. The baseline location of the first scintillator fiber pair is considered at $x = -150$ mm and $z = 3520$ mm (320 mm downstream from the center of the spectrometer). Figure 9 shows a reconstruction of the p_z spectrum for both RF working points of interest, computed through multiple particle tracking simulations. Despite the notoriously good agreements, the reconstruction below does not consider important factors such as scintillator response

and signal acquisition. In addition, this spectral detection is supposed to be relative at the moment. Calibration of the fibers is required for absolute charge measurements and is still under investigation.

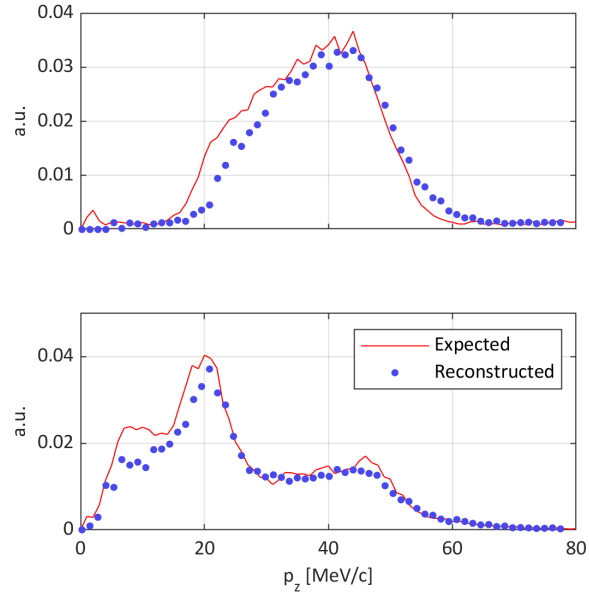


Figure 9: Estimation of p_z reconstruction for $\Phi = (120, -70)$ (top) and $\Phi = (70, -110)$ (bottom). Computed through through 61 ASTRA simulations ranging dipole field strengths from 0 to 0.3 T and scintillator fibers located at $x = -150$ mm and $z = 3520$ mm.

CONCLUSION

This paper introduced the diagnostics for P³ experiment, consisting of an arrangement of broadband pick-ups (BBPs), 2 types of Faraday cups and a variety of scintillating detectors. The BBPs are currently assembled and under test. Preliminary measurements with ≈ 10 ps e- bunches are scheduled before the end of 2023. However, despite their design being less advanced,

despite their technical design is still in progress the Faraday cups were studied in greater detail as they will arguably provide the most accurate detection of the captured e+ charge. Thus we performed a preliminary error study based on simulations, envisaging reasonably high quality measurements of the Faraday cups, specially at RF working points of interest.

ACKNOWLEDGEMENT

This work was done under the auspices of the CHART Collaboration (Swiss Accelerator Research and Technology, <http://www.chart.ch>).

REFERENCES

- [1] E. Prat *et al.*, “A compact and cost-effective hard X-ray free-electron laser driven by a high-brightness and low-energy electron beam”, *Nat. Photonics*, vol. 14, pp. 748–754, 2020. doi: 10.1038/s41566-020-00712-8

- [2] N. Vallis *et al.*, “The P³ Experiment: a Positron Source Demonstrator for Future Lepton Colliders”, 2023.
doi:10.48550/arXiv.2308.16803
- [3] R. H. Helm, “Adiabatic Approximation for Dynamics of a Particle in the Field of a Tapered Solenoid”, SLAC Report No. 4, 1962.
- [4] R. Chehab, “Positron Sources”, in *Proc. Cern Accelerator School, 3rd general accelerator physics course*, Salamanca, Spain, pp. 105-132, CERN, 1988.
doi:10.5170/CERN-1989-005
- [5] ASTRA: A Space Charge Tracking Algorithm,
<https://www.desy.de/~mpyf1o/>.
- [6] 27 GHz SMA Feedthrough for UHV Applications 242-SMAD27G-C16, Allectra GmbH, 2019.
- [7] Microwave 1.85 mm (SMA) feedthrough 242-SMAD65G-C16, Allectra GmbH, 2022.
- [8] 1.85 mm Male to 3.5 mm Male Cable Assemblies, Pasternack Enterprises,
<https://www.pasternack.com/1.85mm-male-to-3.5mm-male-cable-assemblies-category.aspx>
- [9] T. Suwada, M. A. Rehman, and F. Miyahara, “First simultaneous detection of electron and positron bunches at the positron capture section of the SuperKEKB factory”, *Sci. Rep.*, vol. 11, p. 12751, 2021. doi:10.1038/s41598-021-91707-0
- [10] T. Suwada, “Direct observation of positron capture process at the positron source of the superKEKB B-factory”, *Sci. Rep.*, vol. 12, p. 18554, 2022.
doi:10.1038/s41598-022-22030-5
- [11] V. Arsov *et al.*, “Evaluation of the cone-shaped pickup performance for low charge sub-10 fs arrival-time measurements at free electron laser facilities”, *Phys. Rev. Accel. Beams*, vol. 18, p. 012801, 2012.
doi:10.1103/PhysRevSTAB.18.012801
- [12] CST Studio Suite Electromagnetic Simulation Solvers,
<https://www.3ds.com/products-services/simulia/products/cst-studio-suite/solvers/>
- [13] Ansys HFSS, Best-In-Class 3D High Frequency Structure Simulation Software,
<https://www.ansys.com/products/electronics/ansys-hfss>
- [14] C. D. Johnson, “The development and use of alumina ceramic fluorescent screens”, CERN Report No. CERN-PS-90-42-AR, 1990.